Supporting Information for

High Photovoltaic Quantum Efficiency in Ultrathin van der Waals Heterostructures

Joeson Wong[1‡], Deep Jariwala[1,2‡], Giulia Tagliabue[1,4], Kevin Tat[1], Artur R. Davoyan[1,2,3], Michelle C. Sherrott[1,2] and Harry A. Atwater[1,2,3,4]*

[1]Department of Applied Physics and Materials Science, California Institute of Technology, Pasadena, CA-91125, USA

[2]Resnick Sustainability Institute, California Institute of Technology, Pasadena, CA-91125, USA

[3]Kavli Nanoscience Institute, California Institute of Technology, Pasadena, CA-91125, USA

[4]Joint Center for Artificial Photosynthesis, California Institute of Technology, Pasadena, CA-91125, USA

* Corresponding author: Harry A Atwater (haa@caltech.edu)

‡ These authors contributed equally

S1. Optical and Scanning Photocurrent Images of Samples

Optical and scanning photocurrent measurements were taken on all samples analyzed in this work, presented in Figure S1. Sample 1 is the high-performance device for which results are presented in Figure 2 and 3 of the main text. Results presented in Figure 5 and 7 correspond to Sample 2. Figure 6 draws comparisons between Samples 1 and 3, and Figure 4 draws comparisons between Samples 2 and 3.

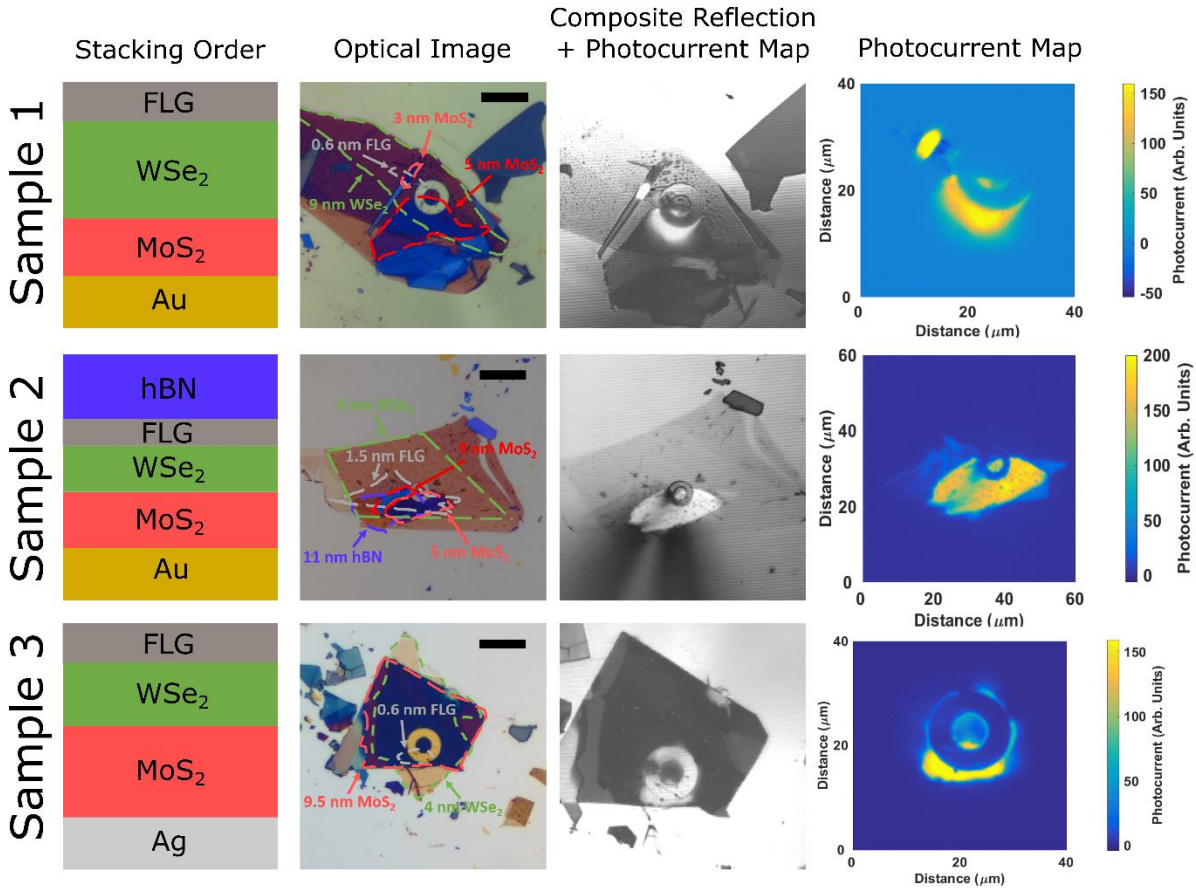

Figure S1. Sample Images: The heterostructure designs, optical images, composite reflection & photocurrent maps, and the photocurrent maps for all the samples analyzed in this paper. The outlines in the optical images correspond to specific materials with the appropriate thickness and materials labeled (scale bar = 20 μm). The composite reflection and photocurrent map is made by superimposing a reflection mode scan with a photocurrent scan ($\lambda = 633$ nm). The bright white regions in the composite image correspond to high photocurrent.

S2. Diode equation fitting and simulated AM 1.5G

A diode model is commonly used to examine the characteristics of photovoltaic devices. Here, we assume a single diode model with a series and shunt resistance as a simple model to understand the photovoltaic device characteristics:

$$I(V) = I_{dark}\left(\exp\left(\frac{q(V - IR_s)}{nk_bT}\right) - 1\right) + \frac{V - IR_s}{R_{sh}} - I_L \qquad (1)$$

where I_{dark} is the dark current, q is the fundamental charge constant (1.602×10^{-19} C), n is the ideality factor, k_b is the Boltzmann constant (1.38×10^{-23} J K^{-1}), T is the thermodynamic temperature (300 K, for this case), R_s is the series resistance, R_{sh} is the shunt resistance, and I_L is the generated current from the photovoltaic effect under illumination. Here, V is the applied voltage and I is the measured current. At short circuit, $V = 0$ and $I \to I_{sc}$. Thus,

$$I_L = I_{dark}\left(\exp\left(\frac{-qI_{sc}R_s}{nk_bT}\right) - 1\right) - \frac{I_{sc}R_s}{R_{sh}} - I_{sc} \qquad (2)$$

For the case $R_s = 0$, we recover the usual expression $I_L = -I_{sc}$. We use the above two

expressions along with the measured short circuit current I_{sc} to perform a four parameter $(n, I_{dark}, R_s, R_{sh})$ fit to the open circuit voltage V_{oc} and the power conversion efficiency $\eta = P_{device}/P_{input}$ as a function of input power. Here, we have explicitly measured the input power of the laser illumination. The fitted parameters are listed in Figure 3 (b) and Figure 3 (c) in the main manuscript, and are used to generate the dashed lines in those plots. Note that we use the same fitted parameters for both data sets. It is also important to note that by fitting the parameters under illumination at various powers, we expect the fitted parameters to represent primarily the device characteristics that are probed by laser illumination, and not all the other devices that are in parallel (which would be the case if we fitted to the dark IV).

To estimate the power conversion efficiency under AM 1.5G illumination for the particular device, we use the expression:

$$I_{sc} = -qA \int_{400\ nm}^{800\ nm} EQE_{exp}(\lambda) S_{AM\ 1.5G}(\lambda) d\lambda \qquad (3)$$

where q is the fundamental charge constant (1.602×10^{-19} C), A is the estimated active area, EQE_{exp} is the experimentally measured EQE for the device, and $S_{AM\ 1.5G}$ is the solar photon flux (photons m^{-2} s^{-1} nm^{-1}). Using the above fitted parameters and the calculated I_{sc}, we can simulate the $I(V)$ characteristics of the device. We take $J(V) = I(V)/A$ and calculate the power conversion efficiency (η) as

$$\eta = \frac{J_m V_m}{\int_0^\infty \left(\frac{hc}{\lambda}\right) S_{AM\ 1.5G}(\lambda) d\lambda} \qquad (4)$$

Where J_m, V_m is the current density and voltage at the maximum power point, respectively, and the denominator of the above expression represents the total incident power of solar irradiation ($S = \int_0^\infty \left(\frac{hc}{\lambda}\right) S_{AM\ 1.5G}(\lambda) d\lambda$ = 1000 W m^{-2}). We plot this as a function of estimated active area A in Figure S2 (a). Note that with increasing estimated active area, we observe an increase in the power conversion efficiency.

Here, the active area effectively reduces the dark current density $J_{dark} = I_{dark}/A$ for increasing A, and therefore leads to a concentration-like effect on the power conversion efficiency. Thus, there is a logarithmic dependence of η on the active area A and therefore η varies weakly with A. Moreover, the above analysis for A also allows us to estimate the appropriate area for the simulated device performance, as this is not the area under illumination, but rather the area from which dark current, series resistance, and shunt resistance contribute to the total measured current (*i.e.* the total sample size). We estimate this area to be in the range of $20^2 - 40^2$ μm^2 from the optical image (Figure S1) and plot the J-V characteristics assuming a 30×30 μm^2 active area below (Figure S2 (b)). Typical photovoltaic figures of merit are also shown. We achieve $J_{sc} > 8$ mA/cm^2 under 1 sun illumination. This value depends only on the experimentally measured EQE and does not depend on any fitting parameters, as evident in Eqn. 3. However, the expected V_{oc} and FF are sub-optimal, due to the type-II band alignment and high series resistance of the device. Thus, despite having fairly large short circuit current densities, device performance is limited primarily by the open circuit voltage and fill fraction, leading to an overall predicted $\eta_{AM\ 1.5G} \approx 0.4\%$.

The above analysis differs from the typical experimental scenario where we estimate the input power as $P_{input} = SA$, where $S = 1000$ W m^{-2} and A is the illumination area. Thus, the experimental efficiency is given as $\eta = \frac{P_{m,exp}}{P_{input}}$, where $P_{m,exp}$ is the maximum power of the experimentally measured device. In the experimental case, A is optimally the solar illumination area through some well-calibrated aperture.[1] In this case, the power conversion efficiency is inversely proportional to the estimated active area and therefore leads to larger J_{sc} and η for smaller A. This is a common source of error in estimating η for small devices, as $|\delta\eta|/\eta = |\delta A|/A$, with the error in efficiency $\delta\eta$ depending linearly with the error in active area estimation δA. Particularly for micron and nano-scale devices such as in van der Waals materials, particular care must be taken to avoid errors in measuring and calculating the power conversion efficiency, as discussed by Snaith *et al.* in ref. 1. Here, we show a distribution of efficiencies based on our active area estimation, leading to AM 1.5G power conversion efficiencies between 0.25% to 0.5%. For our above calculation methodology, we can derive the error dependence to be roughly $\frac{|\delta\eta|}{\eta} \approx \frac{|\delta A|}{A}\left(\frac{nk_bT}{qV_{oc}}\right)$, where the extra factor of $nk_bT/(qV_{oc})$ comes from the dependence of η with an estimated V_{oc}, rather than J_{sc}. The low values of absolute efficiency and logarithmic dependence on active area using our calculation methodology imply a weak dependence of the error on estimated active area, and thus suggests our calculated performance is a reasonable estimate for an experimental AM 1.5G measurement.

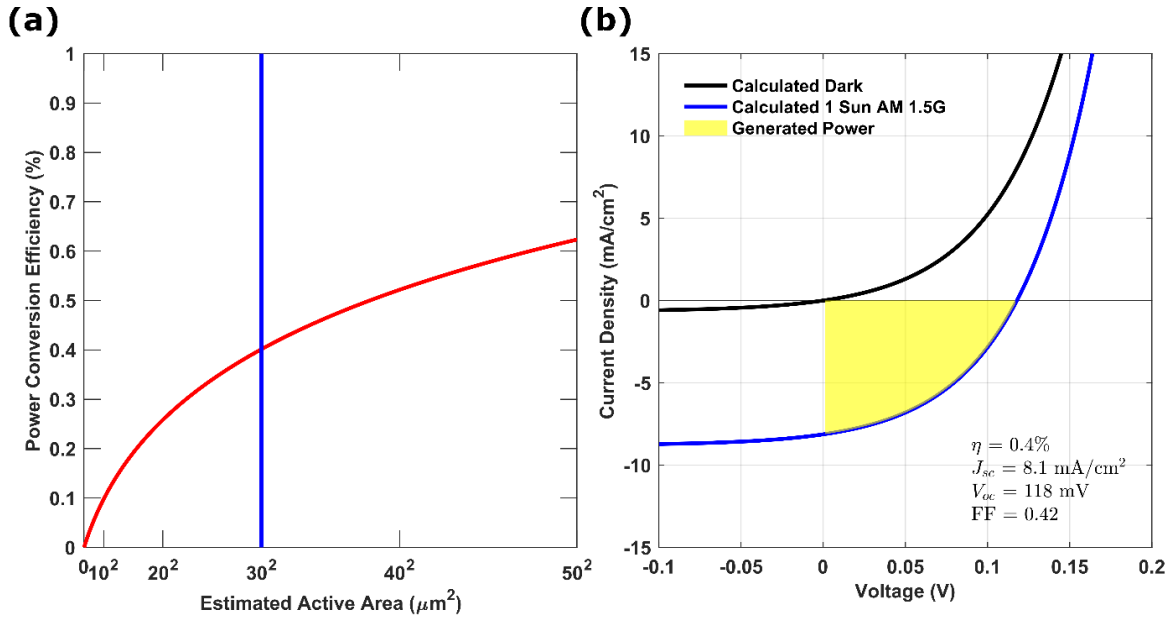

Figure S2. Estimated 1 Sun AM 1.5G performance: **(a)** Estimated 1 Sun AM 1.5G power conversion efficiency of the device measured in Figure 2 and 3 of the main manuscript as a function of estimated active area. The blue line corresponds to a 30×30 μm^2 estimated active area used for the plot in (b). **(b)** The estimated J-V curve of the device studied in Figure 2 and 3 of the main manuscript in the dark (black line) and under 1 Sun AM 1.5G illumination (blue) assuming a 30×30 μm^2 active area. Estimated device characteristics are in the bottom right-hand corner of the plot.

S3. Effective medium theory in ultrathin heterostructures

Given that the samples considered in this work are deep sub-wavelength (~10-15 nm ≪ ~ 500 nm), it is expected that an effective medium theory can be employed. An effective medium dielectric constant was calculated using

$$\varepsilon_{EMT}(\lambda) = \frac{\sum_{j=1}^{N} \varepsilon_j(\lambda) t_j}{\sum_{j=1}^{N} t_j} \quad (5)$$

where ε_{EMT} is the effective medium dielectric constant, ε_j is the dielectric constant of the jth layer, t_j is the thickness of the jth layer, and N is the total number of layers, excluding the metal substrate. Figure S3 (a) shows the effective dielectric constant calculated for the sample studied in Figure 4 (a) and (b) of the main paper. Optically, the dielectric constant can be considered as a single absorbing dielectric layer. The validity of this approach is shown by calculating the absorption spectrum using the effective medium dielectric constant and all the individual dielectric components in a stack (Figure S3 (b)). Thus, one would expect similar non-trivial phase shifts at the absorbing dielectric – metal interface,[2] even when several layers are incorporated. In the deep sub-wavelength regime, the phase shifts between different van der Waals heterostructures are unimportant as the light will average over these effects. Therefore, near-unity absorption is also achievable in ultrathin van der Waals heterostructures, as has been demonstrated for single-component absorbers on a reflective surface.[3]

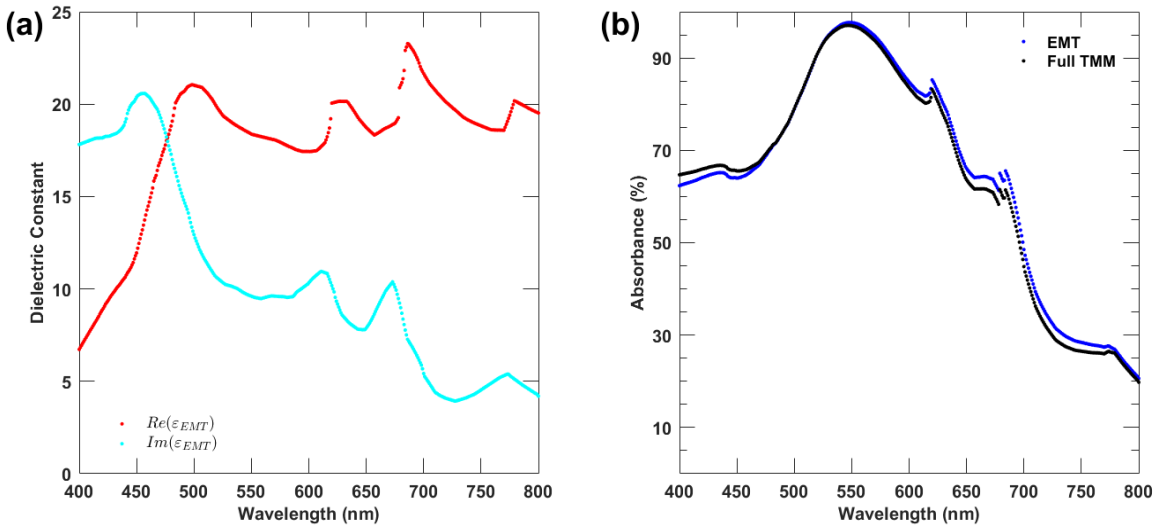

Figure S3. Effective medium theory in ultrathin van der Waals heterostructures: **(a)** The real (red) and imaginary (cyan) part of the effective medium theory (EMT) dielectric constant of the gold sample studied in Figure 4 of the main paper (1.5 nm FLG/4 nm WSe_2/5 nm MoS_2/Au). **(b)** The absorption spectrum calculated using the effective medium dielectric constant (blue dots, 10.5 nm EMT material/Au) versus the absorption spectrum calculated using all the dielectric components (black dots, 1.5 nm FLG/4 nm WSe_2/5 nm MoS_2/Au).

S4. Absorbance and EQE Plots of Thick and Thin PN Junctions

Despite the vastly different absorbance and EQE spectra between the thick and thin pn heterojunction devices (Figure S4), along with the differences in active-layer thicknesses (13 nm and 9 nm, respectively), the active-layer and experimental IQE response of the two devices are comparable (Figure 7 of the main manuscript). This suggests competing effects in the generation and collection of carriers[4–10] in the ultrathin limit. Further experimental studies on carrier transport corroborated with theoretical models are needed to understand the role this may have on ultrathin photovoltaic devices made of van der Waals materials.

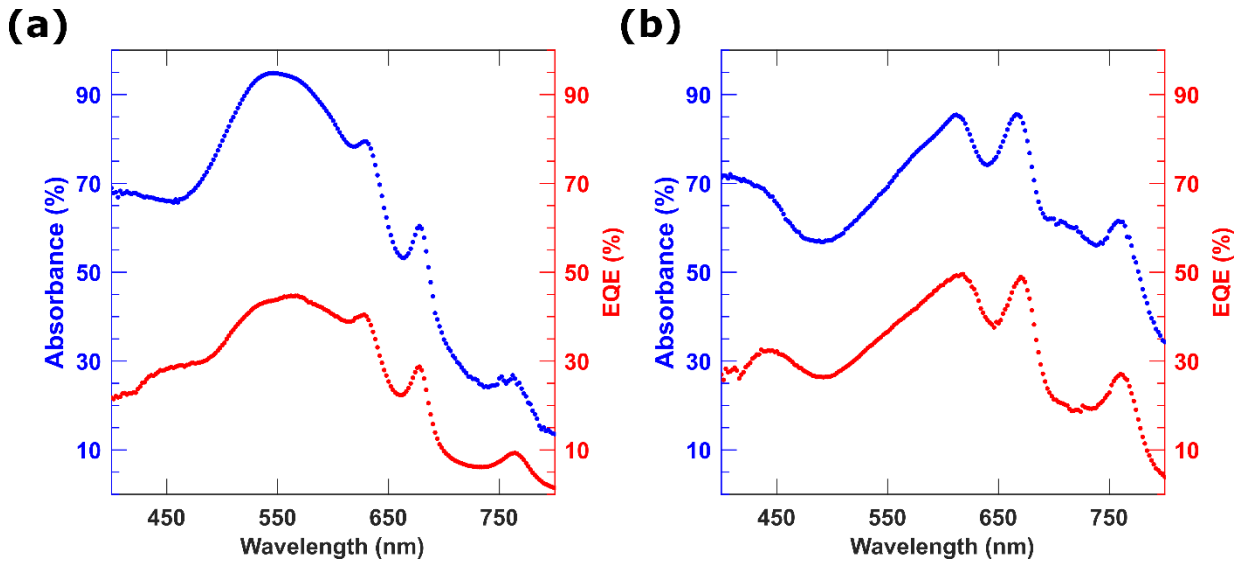

Figure S4. Absorbance and EQE of Thick and Thin PN Junctions: **(a)** Experimentally measured absorbance (blue) and EQE (red) of the thin pn heterojunction (1.5 nm FLG/4 nm WSe_2/5 nm MoS_2/Au). **(b)** Same as in (a) except for a thick pn heterojunction (11 nm hBN/1.5 nm FLG/4 nm WSe_2/9 nm MoS_2/Au).

References

(1) Snaith, H. J. The Perils of Solar Cell Efficiency Measurements. *Nat. Photonics* **2012**, *6*, 337–340.

(2) Kats, M. A.; Blanchard, R.; Genevet, P.; Capasso, F. Nanometre Optical Coatings Based on Strong Interference Effects in Highly Absorbing Media. *Nat. Mater.* **2012**, *12*, 20–24.

(3) Jariwala, D.; Davoyan, A. R.; Tagliabue, G.; Sherrott, M. C.; Wong, J.; Atwater, H. A. Near-Unity Absorption in van Der Waals Semiconductors for Ultrathin Optoelectronics. *Nano Lett.* **2016**, *16*, 5482–5487.

(4) Zhu, X.; Monahan, N. R.; Gong, Z.; Zhu, H.; Williams, K. W.; Nelson, C. A. Charge Transfer Excitons at van Der Waals Interfaces. *J. Am. Chem. Soc.* **2015**, *137*, 8313–8320.

(5) Chen, H.; Wen, X.; Zhang, J.; Wu, T.; Gong, Y.; Zhang, X.; Yuan, J.; Yi, C.; Lou, J.; Ajayan, P. M.; *et al.* Ultrafast Formation of Interlayer Hot Excitons in Atomically Thin MoS_2/WS_2 Heterostructures. *Nat. Commun.* **2016**, *7*, 12512.

(6) Georgiou, T.; Jalil, R.; Belle, B. D.; Britnell, L.; Gorbachev, R. V; Morozov, S. V; Kim, Y.-J.;

Gholinia, A.; Haigh, S. J.; Makarovsky, O.; *et al.* Vertical Field-Effect Transistor Based on Graphene-WS_2 Heterostructures for Flexible and Transparent Electronics. *Nat. Nanotechnol.* **2013**, *8*, 100–103.

(7) Yu, W. J.; Li, Z.; Zhou, H.; Chen, Y.; Wang, Y.; Huang, Y.; Duan, X. Vertically Stacked Multi-Heterostructures of Layered Materials for Logic Transistors and Complementary Inverters. *Nat. Mater.* **2012**, *12*, 246–252.

(8) Bhanu, U.; Islam, M. R.; Tetard, L.; Khondaker, S. I. Photoluminescence Quenching in Gold - MoS_2 Hybrid Nanoflakes. *Sci. Rep.* **2015**, *4*, 5575.

(9) Buscema, M.; Steele, G. A.; van der Zant, H. S. J.; Castellanos-Gomez, A. The Effect of the Substrate on the Raman and Photoluminescence Emission of Single-Layer MoS_2. *Nano Res.* **2014**, *7*, 1–11.

(10) Lee, C.-H.; Lee, G.; van der Zande, A. M.; Chen, W.; Li, Y.; Han, M.; Cui, X.; Arefe, G.; Nuckolls, C.; Heinz, T. F.; *et al.* Atomically Thin PN Junctions with van Der Waals Heterointerfaces. *Nat. Nanotechnol.* **2014**, *9*, 676–681.